Nanoscale

PAPER

Cite this: *Nanoscale*, 2024, **16**, 6618

Phase transition in $WSe_{2-x}Te_x$ monolayers driven by charge injection and pressure: a first-principles study†

Liyuan Chen,[a] Li Chen,[a] Hongli Chen,[a] Kai Jiang,[a] Liangqing Zhu,[a] Liyan Shang,[a] Yawei Li,[a] Shijing Gong[a] and Zhigao Hu*[a,b]

Received 2nd December 2023,
Accepted 26th February 2024

DOI: 10.1039/d3nr06164g

rsc.li/nanoscale

Alloying strategies permit new probes for governing structural stability and semiconductor–semimetal phase transition of transition metal dichalcogenides (TMDs). However, the possible structure and phase transition mechanism of the alloy TMDs, and the effect of an external field, have been still unclear. Here, the enrichment of the Te content in $WSe_{2-x}Te_x$ monolayers allows for coherent structural transition from the H phase to the T′ phase. The crystal orbital Hamiltonian population (COHP) uncovers that the bonding state of the H phase approaches the high-energy domain near the Fermi level as the Te concentration increases, posing a source of structural instability followed by a weakened energy barrier for the phase transition. In addition, the structural phase transition driven by charge injection opens up new possibilities for the development of phase-change devices based on atomic thin films. For $WSe_{2-x}Te_x$ monolayers with the H phase as the stable phase, the critical value of electron concentration triggering the phase transition decreases with an increase in the x value. Furthermore, the energy barrier from the H phase to the T′ phase can be effectively reduced by applying tensile strain, which could favor the phase switching in electronic devices. This work provides a critical reference for controllable modulation of phase-sensitive devices from alloy materials with rich phase characteristics.

Introduction

Compared with bulk materials, two-dimensional materials have unusual properties and good application prospects due to the quantum confinement effect caused by ultra-thin thickness. As an important member of two-dimensional materials, two-dimensional transition metal dichalcogenides (2D TMDs) have attracted extensive attention in the fields of condensed matter physics and materials science because of their unique structure.[1–4] 2D TMDs form a layered structure similar to a sandwich form, with the transition metal atomic layer sandwiched between the two layers of chalcogenide atoms. Chalcogenide atoms and transition metal atoms may exhibit different atomic arrangements, resulting in polymorphism phenomena. Controlling the stability of multi-phase structures with unique properties can be applied to monolayer phase engineering, phase-change memory and other technical fields.[5–9] One of the most explored systems is group VI TMDs, whose molecular formula can be expressed as MX_2 (M = Mo or W, X = S, Se or Te). Polymorphic TMDs include the trigonal prismatic phase (H), the orthorhombic phase (Td) and the octahedral phase (T), while the unstable T phase tends more readily to the distorted octahedral phase (T′). The crystallization of various configurations has rich phase-related research values. For example, the problem of large contact resistance at the interface can be solved based on the transverse heterojunction composed of different phases in the same material.[10–12] Although it has been demonstrated that the transition from the H phase to the T′ phase can be induced by direct chemical exfoliation,[13] lithium embedding,[14] heat treatment,[15] and laser induction,[16] it is still a challenge to achieve reversible structural phase transition between the H- and T′-phases of TMDs. It is found that the structure phase transition of thin atomic layer TMDs can be controlled reversibly and non-destructively by electrostatic gating and tensile strain.[17–19] However, when the energy difference between the two phases is large, a higher level of charge injection and a larger strain are required, so it is difficult to realize the phase transition directly.

[a]*Technical Center for Multifunctional Magneto-Optical Spectroscopy (Shanghai), Engineering Research Center of Nanophotonics & Advanced Instrument (Ministry of Education), Department of Physics, School of Physics and Electronic Science, East China Normal University, Shanghai 200241, China. E-mail: zghu@ee.ecnu.edu.cn; Fax: +86-21-54342933; Tel: +86-21-54345150*

[b]*Collaborative Innovation Center of Extreme Optics, Shanxi University, Taiyuan, Shanxi 030006, China*

† Electronic supplementary information (ESI) available. See DOI: https://doi.org/10.1039/d3nr06164g

Alloying of TMDs provides a possible way to regulate the thermodynamic stability of structures and semiconductor–metal phase transitions.[20–24] In 2016, Li *et al.* found that the transition gate voltage of the $W_xMo_{1-x}Te_2$ monolayer can be reduced arbitrarily by alloying by developing a new density functional-based method.[18] In 2019, the direct synthesis of monolayer H- and T′-phase $WTe_{2x}S_{2(1-x)}$ alloys by one-step chemical vapor deposition (CVD) was reported.[25] Also, a continuous structural phase transition from Td to T′ to H polytype was demonstrated by increasing the Se concentration in Se-substituted $MoTe_2$ thin films.[26] In 2021, the synthesis of $Mo_xW_{1-x}Te_2$ with controllable thickness and chemical composition ratios by the CVD method was demonstrated.[27] The above studies show that transition metal telluride alloys have great potential in the application of phase-sensitive devices. The monolayer WTe_2 is predicted to be a new class of two-dimensional quantum spin Hall insulators,[28] whose stable phase is the T′ phase at room temperature.[29–31] Interestingly, except for WTe_2, the thermodynamically stable phase of MX_2 under ambient conditions belongs to the semiconductor H phases. Therefore, it is reasonable to search for WTe_2 alloy members to achieve the same thermodynamic stability of the H phase and the T′ phase, which will bring new physical properties. Monolayer WSe_2 exhibits exciton valley polarization and valley coherence,[32,33] and exists as the stable H phase at room temperature,[6,34] making it a preferred component of alloy materials. The synthesis of monolayer $WSe_{2(1-x)}Te_{2x}$ alloys by chemical vapor transport (CVT) has been demonstrated experimentally.[35] However, the structure, phase transition mechanism and regulation method have been still unclear due to the incompatibility of the phase. In addition to thermodynamics, the transition barrier is also important. To some extent, the transition barrier can qualitatively reflect the kinetics or rate. The lower the energy barrier, the faster the transition rate, and the higher the sensitivity of the device. Based on monolayer $WSe_{2-x}Te_x$ alloys, we can further regulate the thermodynamic stability of the H-phase and T′-phase and the energy barrier between the two phases by injecting charge and applying strain, respectively, which can be applied to phase-change storage technology.

In this work, the structural transition from the H phase to the T′ phase of monolayer $WSe_{2-x}Te_x$ alloys has been studied by using the first principles calculation method based on density functional theory (DFT). The thermodynamics and phase transition kinetics are analyzed mainly from the two aspects of free energy and energy barrier to elucidate the mechanism of phase transition. The results show that the stable phase of $WSe_{2-x}Te_x$ monolayers changes from H to T′ with increasing the Te concentration, and the transition energy barrier between the two phases decreases gradually. In addition, for the monolayer $WSe_{2-x}Te_x$ with the H phase as the stable phase, the H to T′ phase transition can be achieved by electron injection. It was found that the critical electron concentration decreases upon increasing the Te concentration. Moreover, the transition energy barrier from the H phase to the T′ phase can be reduced by applying tensile strain, especially in the application of large strain conditions. This work presents a detailed comprehension of controllable modulation on the phase transitions for $WSe_{2-x}Te_x$ monolayers, which can push the phase-sensitive electronic device applications.

Calculation details

DFT calculations employ the projector augmented (PAW) wave method[36] as implemented in the Vienna *ab initio* simulation package (VASP).[37,38] The electronic exchange–correlation energy was treated by the generalized-gradient approximation of Perdew–Burke–Ernzerhof (GGA-PBE).[39] A cutoff energy of 600 eV was used for the plane-wave basis set. The lattice constants of monolayer $WSe_{2-x}Te_x$ alloys were optimized by the conjugate gradient algorithm. A vacuum layer of more than 15 Å was added in the z direction to avoid spurious interactions between adjacent layers under periodic boundary conditions. The convergence threshold for structural optimization was set to be 10^{-6} eV in energy and 0.01 eV $Å^{-1}$ in force. The k-mesh of 21 × 15 × 1 was performed for the Brillouin-zone integrations in optimization and 31 × 25 × 1 in self-consistency.

To find the change in atomic displacement and the energy barrier in the phase transition from H to T′, the climbing-image nudged elastic band (CI-NEB) method *via* transition state tools (VTST) as implemented in the VASP was used.[40] The phonon dispersion spectrum was calculated by the density functional perturbation theory (DFPT) method using the PHONOPY code in order to further understand the process of phase transition being triggered. The crystal orbital Hamiltonian population (COHP) was analyzed using the LOBSTER package.[41]

Results and discussion

The structures and thermodynamic stability

The atomic structures of the H- and T′-phases of $WSe_{2-x}Te_x$ monolayers are shown in Fig. 1a. In the H- and T′-phases, the six Se (Te) atoms around W are arranged in trigonal prismatic and distorted octahedral structures, respectively. In order to visually understand the phase stability of the H- and T′-phases from $WSe_{2-x}Te_x$ monolayers upon increasing the Te concentration, we select a rectangular unit cell composed of two formula units as the research object, and consider the cases of x = 0, 0.5, 1, 1.5 and 2. After optimized relaxation, the stable geometric structural parameters of $WSe_{2-x}Te_x$ monolayers are shown in Table 1 and Fig. S1.† The lattice constants are 3.316 Å and 5.743 Å in the a and b directions for the monolayer H-WSe_2, which is consistent with the reported values.[11,42,45] Because the radius of the Te ion is larger than that of the Se ion, the bond length of the W–Te bond is longer than that of the W–Se bond. It can allow the lattice constants of both H and T′ phases to expand upon increasing the Te concentration.

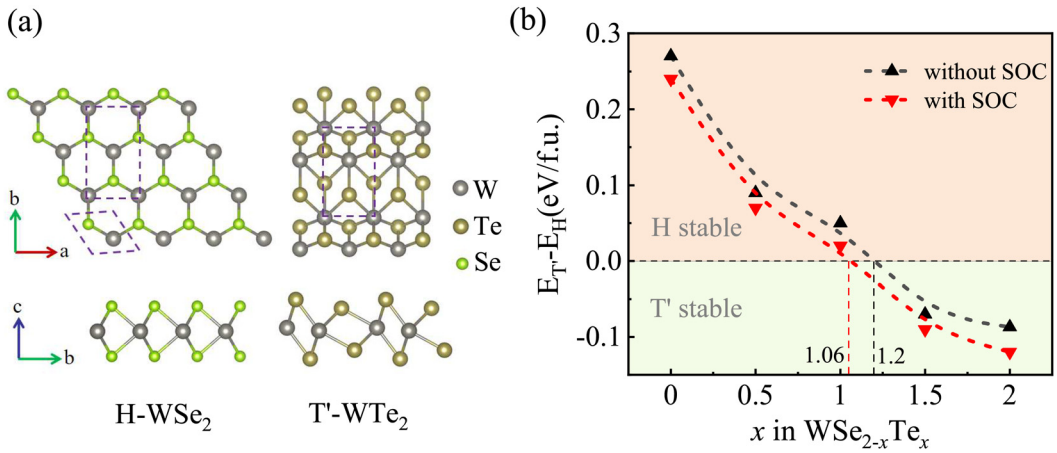

Fig. 1 (a) Structural phases of $WSe_{2-x}Te_x$. Top and side views of monolayer H-WSe_2 and monolayer T′-WTe_2. (b) The phase energy difference $\Delta E = E_{T'} - E_H$ of $WSe_{2-x}Te_x$ monolayers as a function of the Te composition.

Table 1 The equilibrium energy differences and lattice constants of the H- and T′-phases calculated by the PBE method is listed. Note that the lattice parameters *a* and *b* are taken from the rectangular unit cell consisting of two formula units

	H (σ = 0) (eV per MX_2)		Lattice [*a*, *b*](Å)	
Materials	H	T′	H	T′
WSe_2	0	0.27	[3.316, 5.743] [3.315, 5.744][42]	[3.298, 5.944] [3.300, 5.944][42]
$WSe_{1.5}Te_{0.5}$	0	0.09	[3.374, 5.832]	[3.335, 6.099]
WSeTe	0	0.05	[3.431, 5.971]	[3.386, 6.121]
$WSe_{0.5}Te_{1.5}$	0	−0.07	[3.492, 6.041]	[3.428, 6.287]
WTe_2	0	−0.09	[3.552, 6.152] [3.554, 6.152][43]	[3.489, 6.314] [3.498, 6.338][44]

The relative energy stability between the H- and T′-phases of the $WSe_{2-x}Te_x$ monolayers is characterized by the energy difference per formula unit ($\Delta E = E_{T'} - E_H$). If ΔE is negative, it means that the T′ phase is more stable, and *vice versa* in favor of the H phase. In addition, considering that the structure contains atoms with larger atomic numbers, spin–orbit coupling (SOC) is considered in the calculation process for comparison, as shown in Fig. 1b. At lower Te concentrations, the value of ΔE is positive, indicating that the H phase is dominant. The energy difference between the H and T′ phases decreases upon increasing the Te concentration. The two phases coexist when the concentration reaches a certain value. Considering the two conditions with and without SOC, the energy of the two phases is equal at x = 1.06 and 1.2, respectively. When the Te concentration exceeds this critical value, the T′ phase begins to dominate, and the energy difference increases with an increase in the Te concentration. When SOC calculation is not included, the energy differences between the H- and T′-phases of WSe_2 and WTe_2 are 0.27 eV and 0.09 eV, which is consistent with the previous results.[19,23] It is noteworthy that the low energy difference in a certain Te concentration range is consistent with the observed two-phase coexistence in the experiment.[35,46] Considering that the calculation of the PBE+SOC method requires a large amount of system resources and calculation time, and the calculation results of the PBE method are in good agreement with the energy variation trend of the two phases in the experiment, we ignore the effect of SOC interaction in the following calculation.

In order to further investigate the phase stability and possible phase transitions of monolayer $WSe_{2-x}Te_x$ alloys, *ab initio* molecular dynamics (AIMD) simulations were performed at room temperature for both the H phase and the T′ phase. The free energy fluctuation curves at room temperature show that all phases are thermally stable, and the energy order indicates that the stable phase of WTe_2 is the T′ phase, whereas that of WSe_2 prefers the H phase, as shown in Fig. S2.† At the same time, AIMD simulations were also carried out at the growth temperature to check whether the H-$WSe_{2-x}Te_x$ monolayers with a high Te concentration would undergo phase transitions or structural deformation at higher temperatures. By tracking the evolution of the W–W bond length in the temperature range of 300 K to 1100 K and the variation trend of the potential energy surface at 1100 K, the feasibility of phase transitions of monolayer $WSe_{2-x}Te_x$ alloys with a high Te concentration under a continuous hot bath at a high temperature is demonstrated (see Fig. S3† for more details). In addition, the electron band structures of the H- and T′-$WSe_{2-x}Te_x$ monolayers along the high symmetric points are calculated for subsequent analysis, as shown in Fig. S4.† The H phases of WSe_2 and WTe_2 monolayers are both direct band gap semiconductors. Their valence band maximum (VBM) and the conduction band minimum (CBM) are located between the Γ and X points, while the structures of the T′ phase are semi-metallic, which is consistent with the previous reports.[42,44,47] For x = 0.5 and 1, the T′-$WSe_{2-x}Te_x$ monolayers open up a narrow band gap. The band gap decreases upon increasing the Te concentration in H-$WSe_{2-x}Te_x$ monolayers.

The kinetics of structural phase transition

The transition barrier can provide some qualitative insights into what the kinetics or rates may be. In order to obtain the

energy barrier of phase transition from H to T′, the CI-NEB method was used to calculate the potential energy curves of different alloy structures along phase transition coordinates. The energy barriers during the forward and backward phase transition process of $WSe_{2-x}Te_x$ monolayers from the H phase to the T′ phase were calculated. The phase transition paths with the lowest energy barrier are shown in Fig. 2a. Since the Te (Se) atom needs to pass through the center between the two W atoms during the H to T′ phase transition, there is an energy barrier. For the case of x = 0, the energy barrier of the H to T′ phase transition is 1.20 eV, while the energy barrier of the backward transition is 0.93 eV. Upon increasing the Te concentration, the T′ phase becomes more stable and the energy barrier of the H to T′ phase transition decreases gradually. The illustration in Fig. 2a shows the atomic displacement changes during the H to T′ phase transition at x = 1. In order to further understand how the phase transition from H to T′ is triggered, we calculate the phonon dispersion of the H-WSeTe monolayer and the vibration modes at the Γ point associated with the phase transition, as shown in Fig. 2b. Based on the D_{3h} point group, the irreducible representation of the phonon vibration mode of the H phase at the Γ point is expressed as $\Gamma_H = E'' + A'_1 + E' + A''_2$,[48,49] and the corresponding phonon vibration modes are shown on the right panel. From the changes in the atomic positions in the H to T′ phase transformation path in Fig. 2a, it can be found that the phase transformation is mainly related to the displacement of chalcogenide atoms along the b direction, which has a strong correlation with the vibration of the E′ mode. The results are informative for manipulating the phase transition rate of phase-sensitive devices *via* tailoring the Te concentration in experimental observations, which is, however, rarely reported in the contributions of others.

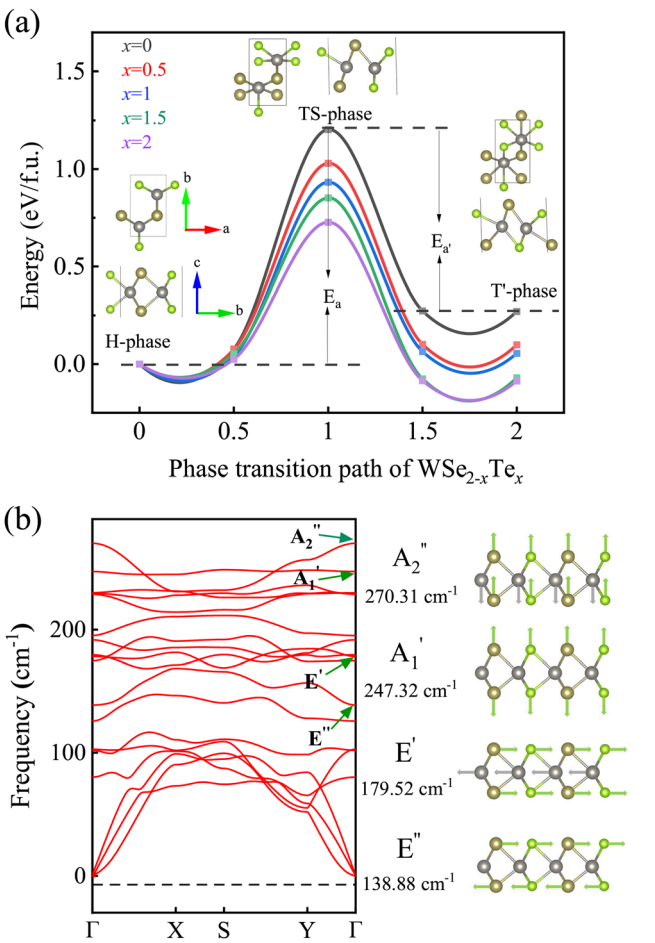

Fig. 2 (a) The free energy curves along the transition path from the H to T′ phases of $WSe_{2-x}Te_x$ monolayers, and the illustration shows the atomic displacement during structural phase transition from the H to T′ phase of the $WSe_{2-x}Te_x$ monolayer at x = 1. E_a and E'_a represent the energy barriers for the forward and backward transitions, respectively. (b) Phonon dispersion of the $WSe_{2-x}Te_x$ monolayer at x = 1 and vibrational modes for optical phonons at the Γ point.

The COHP[50,51] bonding analysis is performed to further understand the reason why the energy barrier of phase transition decreases upon increasing the Te concentration. As shown in Fig. 3, the COHP curves show the bonding and antibonding contributions of the W–Se and W–Te bonds. We can judge the stability of H-$WSe_{2-x}Te_x$ monolayer structures from the energy displacement of bonding states. For the case of x = 0, the bonding state of WSe_2 is distributed in the energy range of −1.17 eV to −6.34 eV. Upon increasing the Te concentration, the bonding state moves towards the Fermi level and distributes at a higher energy. Until x = 2, the bonding state distribution of WTe_2 is between −0.88 eV and −6.06 eV, the higher energy leads to structural instability. Similarly, the integrated projected COHP (IpCOHP) value at the Fermi level decreases gradually upon increasing the Te concentration. It is shown that the H phase bond energy decreases upon increasing the Te concentration, resulting in a decrease in the energy barrier of H to T′ phase transition. Based on the energy difference and energy barrier of the two phases, we believe that the optimal x-value range of the Te concentration of the $WSe_{2-x}Te_x$ monolayer in phase-change devices is between 1 and 1.5.

The effect of electron and hole injection

The transition between different phases of TMDs has always been a hot and difficult problem in the fields of materials science and physics. Several studies have shown that charge injection can induce the phase transition from the H phase to the T′ phase in 2D MX_2 monolayers.[52–55] Previous efforts, however, merely described the phenomenon of charge injection-induced phase transitions, while the microscopic mechanisms and regularities involved are rather speculative. In particular, the charge injection modulation of alloy materials is rarely studied. Based on monolayer $WSe_{2-x}Te_x$ alloys, the effect of injected electron or hole concentrations of 0.0–1.0 e per f.u. and 0.0–1.0 h per f.u. on the relative stability of H and T′ structures was investigated, as shown in Fig. 4. The electron and hole doping are simulated by adding and removing the electron, and the background charge is added to keep the charge neutrality,[56] which is done by soaking the original charged supercell in a jellium background to achieve a net charge of zero.[57] The added electrons were placed in empty states with

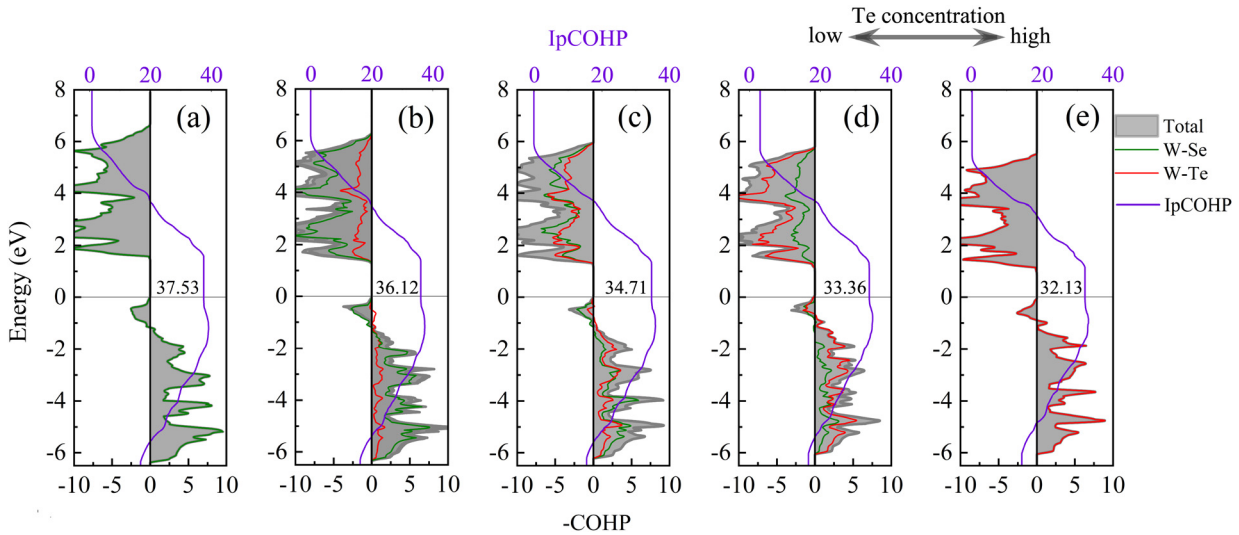

Fig. 3 (a–e) Crystal orbital Hamilton population (COHP) bonding analysis of the H-$WSe_{2-x}Te_x$ monolayers from x = 0 to x = 2. The integrated projected COHPs (IpCOHPs, which indicate the total bond strength) are shown as purple lines, and those integrated up to the Fermi energy are shown with numbers.

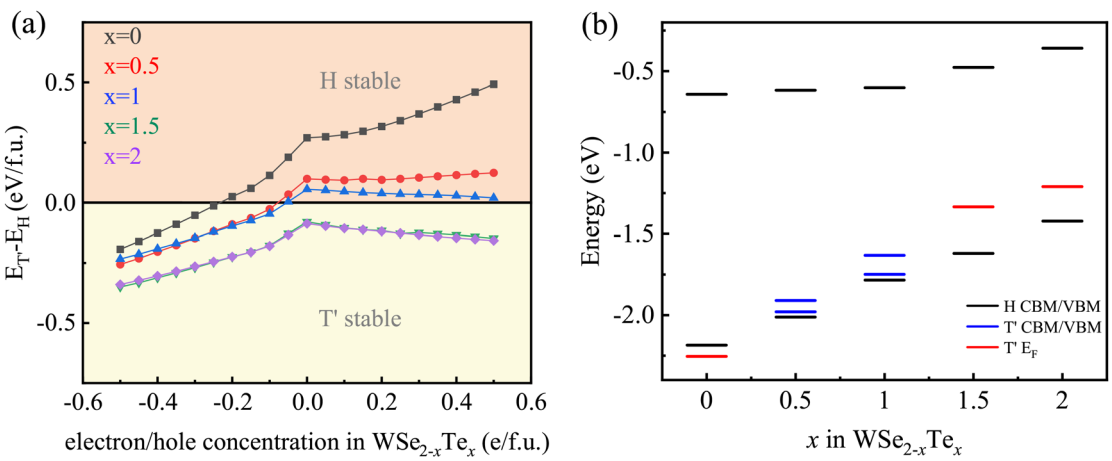

Fig. 4 (a) Energy difference between the H- and T′-phases of $WSe_{2-x}Te_x$ monolayers as a function of the doping electron and hole concentration. (b) The VBM, CBM, and Fermi level (E_F) of $WSe_{2-x}Te_x$ monolayers at different Te concentrations.

the Fermi distribution. The results show that for the case of $x \leq 1$, the H phase is more stable than the T′ phase under charge neutral conditions. With the injection of electrons, the energy difference between the two phases decreases. When the injected electron concentration exceeds a certain critical value, the T′ phase begins to dominate. The critical value decreases with an increment of the Te atom concentration, indicating that phase transition is easy to occur. The effect of hole injection on the relative stability of the H phase and the T′ phase is not obvious. The explanation can be given from the distribution of the VBM and CBM of the semiconductor and the Fermi level of semi-metals in $WSe_{2-x}Te_x$ monolayers at the vacuum level, as shown in Fig. 4b. For the two different cases where the H phase is more stable and the T′ phase is more stable, x = 0.5 and x = 1.5 are further shown in Fig. 5. For the case of x = 0.5, the energy of the H phase is lower than that of the T′ phase. The energy of both phases increases once the charge is injected. The excess electrons will fill the conduction band of the semiconductor H phase, which has a significantly higher energy than that of the T′ phase. Thus, the energy of the H phase increases faster than that of the T′ phase, and the T′ phase becomes more stable with the injection of electrons.

On the other hand, there is little difference in the VBM between the H phase and the T′ phase at x = 0.5. With the injection of holes, the two phases have almost the same priority, and as a result, the energy difference curve of the two phases changes relatively gently. Similarly, for the case of x = 1.5, the T′ phase is the most stable phase, and the Fermi level of the T′ phase is lower than the CBM of the H phase. With the injection of electrons, the energy difference between the two

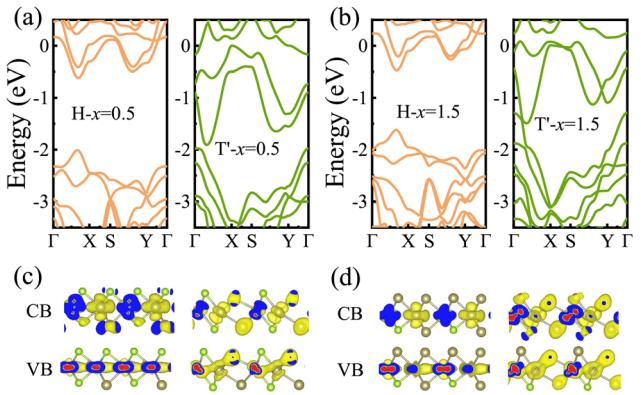

Fig. 5 (a and b) The band structures of $WSe_{2-x}Te_x$ monolayers at x = 0.5 and x = 1.5 in the H phase and T′ phases, respectively. (c and d) The electron densities of the electronic states of the H and T′ phases at x = 0.5 and the H phase at x = 1.5 in the energy range of 0–0.3 eV above the CBM and 0–0.3 eV below the VBM, and those of the T′ phase at x = 1.5 in the energy range of 0–0.3 eV above and below the Fermi level. The values of the isosurface for x = 0.5 and x = 1.5 are set to 0.0008 and 0.0009, respectively.

phases increases and the T′ phase becomes more stable. Since the available states near the Fermi level of the T′ phase are higher than the VBM of the H phase, the injection of holes also induces the T′ phase to be more stable. Fig. 5c and d show the charge density distribution near the CBM and VBM of $WSe_{2-x}Te_x$ monolayers at x = 0.5 and x = 1.5, which is not conducive to electron and hole recombination. It can be seen that for $WSe_{2-x}Te_x$ monolayers with the H phase as the stable phase in Fig. 4b. As the concentration of Te increases, the energy level of the T′ phase that can be filled by the injected electrons increases faster than that of the H phase. Therefore, the slope of the energy difference curve decreases slightly with increasing the Te concentration. However, according to thermodynamic stability, for the case of $x \leq 1$, the decrease of the two-phase energy difference in $WSe_{2-x}Te_x$ monolayers upon increasing the Te concentration is the main reason for the decrease of the critical electron concentration inducing the H to T′ phase transition.

The effect of biaxial tensile strain

Reduction of energy barriers is an important aspect of research when the energy difference between the two phases is held constant. The previous attempts have demonstrated that pressure is a very attractive modulator for phase engineering.[58–61] In particular, the temperature of H–T′ phase transition of thin film $MoTe_2$ is reduced to room temperature by introducing tensile strain experimentally.[62] Whether the tensile strain is effective in regulating the energy barrier between different phases of monolayer TMDs needs further theoretical exploration. The effect of biaxial strain on the transition energy barrier of $WSe_{2-x}Te_x$ monolayers with different Te concentrations has been investigated. The diagram of the biaxial tensile strain applied is shown in the upper panel of Fig. 6b. The biaxial strain is defined as $\varepsilon = (C - C_0)/C$, where C_0 and C represent the lattice constants in the direction of the a and b axes under unstrained and strained conditions,

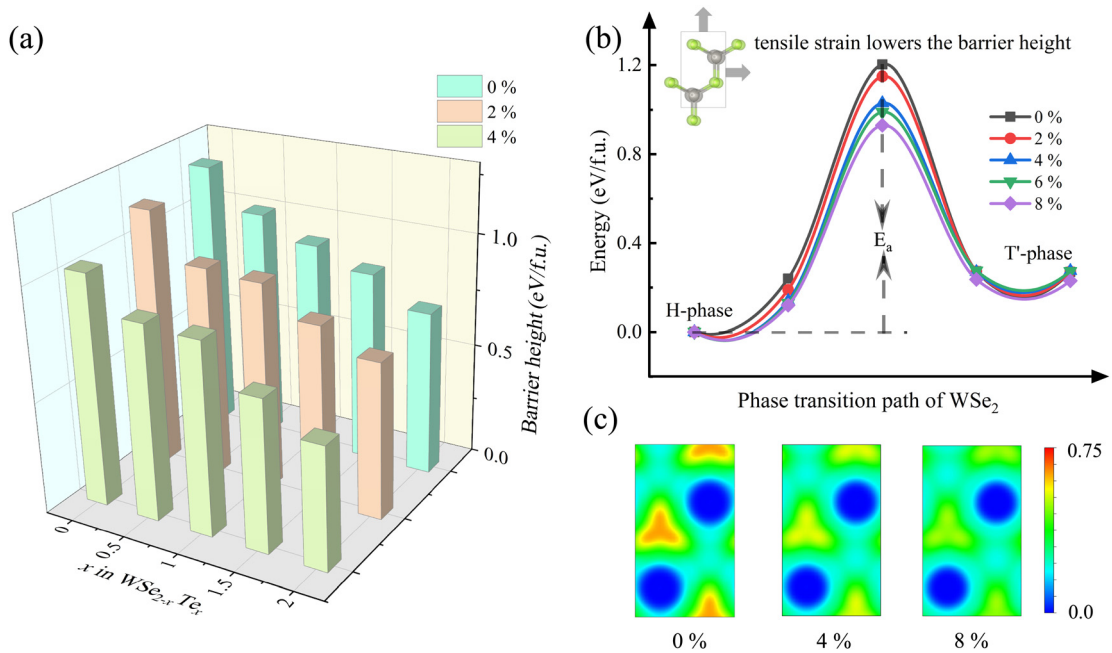

Fig. 6 (a) The forward energy barrier of $WSe_{2-x}Te_x$ monolayers as a function of the Te concentration under 0%, 2% and 4% tensile strain. (b) Schematic view of the phase transition barrier of the $WSe_{2-x}Te_x$ monolayer at x = 0 modulated by the strain. Under tensile strain, the activation energy of the phase transition is lowered, resulting in a faster phase transition rate. (c) The electron localization function (ELF) of the H-phase $WSe_{2-x}Te_x$ monolayer at x = 0 under 0%, 4% and 8% tensile strain, respectively.

respectively. Fig. 6a shows the barrier height of the forward transition from the H phase to the T′ phase for the $WSe_{2-x}Te_x$ monolayers under biaxial tensile strains of 0%, 2% and 4%. The results show that biaxial tensile strain can effectively reduce the barrier height of H to T′ phase transition. For the case of $x = 0$ with better convergence, we further calculated the potential energy curves under 0% to 8% tensile strain, as shown in Fig. 6b. Obviously, the energy barrier height decreases gradually with an increase of the tensile strain, and the energy barrier decreases from 1.20 eV to 0.93 eV under 8% strain, which can further accelerate the phase transition and improve the device sensitivity. To verify the above results, we calculate the electron localization function (ELF) of the H-WSe_2 monolayer under 0%, 4% and 8% strains, as shown in Fig. 6c. The ELF data clarify the degree of electronic localization and can be used to analyze bonding properties. We cut along the *c*-axis with the W atom as the boundary. Under unstrained conditions, the electron states are distributed in a triangular state between adjacent Te atoms, indicating the existence of covalent bonds. With the increase of strain, the bond length increases and the distribution of electron states between atoms becomes delocalized, which leads to the weakening of bond energy between atoms and is conducive to the occurrence of phase transition. In addition, in order to confirm the feasibility of the above-mentioned methods for regulating the phase transition of TMD alloys, the effects of charge injection on the phase stability and the tensile strain on the energy barrier of $MoSe_{2-x}Te_x$ monolayers and $WSe_{2-x}S_x$ monolayers have been further investigated, as shown in Fig. S5.† Electron injection drives the transition from the H phase to the T′ phase more efficiently, and tensile strain is a feasible way to reduce the energy barrier of phase transition. Therefore, our results have a certain reference value for accelerating phase transitions by charge injection and tensile strain for TMD alloys.

Conclusions

In summary, the phase transition behavior from the H phase to the T′ phase of $WSe_{2-x}Te_x$ monolayers has been systematically investigated using DFT calculations. The ratio of Te atoms to Se atoms determines the thermodynamically stable phase of the $WSe_{2-x}Te_x$ monolayers. At lower Te concentrations, the H phase is more stable than the T′ phase. Then, upon increasing the Te concentration, the thermally stable phase begins to transition from the H phase to the T′ phase. Interestingly, the energy barrier of the H to T′ phase transition in the $WSe_{2-x}Te_x$ monolayers decreases upon increasing the Te concentration. The COHP bonding analysis shows that the increment of Te concentration causes the bonding state of the H phase to move to a higher level close to the Fermi level, which makes the structure unstable and easier to trigger phase transition. In addition, for $WSe_{2-x}Te_x$ monolayers with the H phase as the stable phase, the phase transition from the H phase to the T′ phase can be triggered when the electron injection exceeds a certain concentration and the critical value of electron injection decreases upon increasing the Te concentration. More importantly, the mechanism of phase transition induced by charge injection of $WSe_{2-x}Te_x$ alloys has been further explained, which is conducive to grasping the regularity of charge injection induced phase transition in the future study. On the other hand, biaxial tensile strain can effectively reduce the barrier height of the H to T′ phase transition in $WSe_{2-x}Te_x$ monolayers, resulting in effective regulation of the phase transition rate. Therefore, the present research expands the knowledge of the physics associated with TMD phases and will stimulate more innovative phase engineering applications of TMD materials.

Author contributions

L. Y. Chen initiated and performed the calculations and wrote the manuscript. L. Y. Chen, L. Chen and Z. G. Hu discussed the underlying mechanism of the manuscript. H. L. Chen, K. Jiang and L. Q. Zhu provided the computational resources. L. Y. Shang, Y. W. Li and S. J. Gong gave a detailed analysis of the theoretical data. All authors discussed the results and commented on the manuscript.

Conflicts of interest

The authors declare no competing financial interest.

Acknowledgements

This work was financially supported by the National Natural Science Foundation of China (grant no. 62090013, 61974043, and 61974044), the National Key Research and Development Program of China (grant no. 2019YFB2203403), the Projects of Science and Technology Commission of Shanghai Municipality (grant no. 21JC1402100), and the Program for Professor of Special Appointment (Eastern Scholar) at Shanghai Institutions of Higher Learning.

References

1 N. Mondal, N. Azam, Y. N. Gartstein, M. MahjouriSamani and A. V. Malko, *Adv. Mater.*, 2022, **34**, 2110568.
2 Z. Lai, Y. Yao, S. Li, L. Ma, Q. Zhang, Y. Ge, W. Zhai, B. Chi, B. Chen, L. Li, L. Wang, Z. Zheng, L. Gu, Y. Du and H. Zhang, *Adv. Mater.*, 2022, **34**, 2201194.
3 B. Zhou, A. Y. Cui, L. C. Gao, K. Jiang, L. Y. Shang, J. Z. Zhang, Y. W. Li, S.-J. Gong, Z. G. Hu and J. H. Chu, *Phys. Rev. Mater.*, 2021, **5**, 125404.
4 B. Zhou, K. Jiang, L. Y. Shang, J. Z. Zhang, Y. W. Li, L. Q. Zhu, S.-J. Gong, Z. G. Hu and J. H. Chu, *J. Mater. Chem. C*, 2020, **8**, 11160.

5 Y. Wang, J. Xiao, H. Zhu, Y. Li, Y. Alsaid, K. Y. Fong, Y. Zhou, S. Wang, W. Shi, Y. Wang, A. Zettl, E. J. Reed and X. Zhang, *Nature*, 2017, **550**, 487.

6 W. Liu, S. Li, H. Wu, N. Dhale, P. Koirala and B. Lv, *Phys. Rev. Mater.*, 2021, **5**, 014802.

7 S. Park, C. Kim, S. O. Park, N. K. Oh, U. Kim, J. Lee, J. Seo, Y. Yang, H. Y. Lim, S. K. Kwak, G. Kim and H. Park, *Adv. Mater.*, 2020, **32**, 2001889.

8 W. Liu, M. R. Osanloo, X. Wang, S. Li, N. Dhale, H. Wu, M. L. Van de Put, S. Tiwari, W. G. Vandenberghe and B. Lv, *Phys. Rev. B*, 2021, **104**, 024507.

9 L. Chen, L. Wang, K. Jiang, J. Z. Zhang, Y. W. Li, L. Y. Shang, L. Q. Zhu, S. J. Gong and Z. G. Hu, *J. Phys. Chem. Lett.*, 2023, **14**, 5760.

10 R. Ma, H. Zhang, Y. Yoo, Z. P. Degregorio, L. Jin, P. Golani, J. G. Azadani, T. Low, J. E. Johns, L. A. Bendersky, A. V. Davydov and S. J. Koester, *ACS Nano*, 2019, **13**, 8035.

11 Y. Zheng, D. Xiang, J. Zhang, R. Guo, W. Wang, T. Liu, L. Loh, Y. Wang, J. Gao, C. Han, M. Bosman, Z. Ni and W. Chen, *Nano Res.*, 2021, **14**, 2703.

12 Y. Yoo, Z. P. DeGregorio, Y. Su, S. J. Koester and J. E. Johns, *Adv. Mater.*, 2017, **29**, 1605461.

13 J. Peng, Y. Liu, X. Luo, J. Wu, Y. Lin, Y. Guo, J. Zhao, X. Wu, C. Wu and Y. Xie, *Adv. Mater.*, 2019, **31**, 1900568.

14 X. Ji, D. Ding, X. Guan, C. Wu, H. Qian, J. Cao, J. Li and C. Jin, *ACS Nano*, 2021, **15**, 15039.

15 L. Liu, J. Wu, L. Wu, M. Ye, X. Liu, Q. Wang, S. Hou, P. Lu, L. Sun, J. Zheng, L. Xing, L. Gu, X. Jiang, L. Xie and L. Jiao, *Nat. Mater.*, 2018, **17**, 1108.

16 H. Ryu, Y. Lee, J. H. Jeong, Y. Lee, Y. Cheon, K. Watanabe, T. Taniguchi, K. Kim, H. Cheong, C.-H. Lee and G.-H. Lee, *Small*, 2023, **19**, 2205224.

17 Y. Sun, Z. Shuai and D. Wang, *Nanoscale*, 2018, **10**, 21629.

18 Y. Li, K.-A. N. Duerloo, K. Wauson and E. J. Reed, *Nat. Commun.*, 2016, **7**, 10671.

19 C. Zhang, S. Kc, Y. Nie, C. Liang, W. G. Vandenberghe, R. C. Longo, Y. Zheng, F. Kong, S. Hong, R. M. Wallace and K. Cho, *ACS Nano*, 2016, **10**, 7370.

20 H. Huang, J. Zha, S. Li and C. Tan, *Chin. Chem. Lett.*, 2022, **33**, 163.

21 Z. Wang, J. Sun, H. Wang, Y. Lei, Y. Xie, G. Wang, Y. Zhao, X. Li, H. Xu, X. Yang, L. Feng and X. Ma, *Appl. Surf. Sci.*, 2020, **504**, 144371.

22 X. J. Yan, Y. Y. Lv, L. Li, X. Li, S. H. Yao, Y. B. Chen, X. P. Liu, H. Lu, M. H. Lu and Y. F. Chen, *Appl. Phys. Lett.*, 2017, **110**, 211904.

23 K.-A. N. Duerloo and E. J. Reed, *ACS Nano*, 2016, **10**, 289.

24 D. Rhodes, D. A. Chenet, B. E. Janicek, C. Nyby, Y. Lin, W. Jin, D. Edelberg, E. Mannebach, N. Finney, A. Antony, T. Schiros, T. Klarr, A. Mazzoni, M. Chin, Y. Chiu, W. Zheng, Q. R. Zhang, F. Ernst, J. I. Dadap, X. Tong, J. Ma, R. Lou, S. Wang, T. Qian, H. Ding, R. M. Osgood Jr., D. W. Paley, A. M. Lindenberg, P. Y. Huang, A. N. Pasupathy, M. Dubey, J. Hone and L. Balicas, *Nano Lett.*, 2017, **17**, 1616.

25 B. Tang, J. Zhou, P. Sun, X. Wang, L. Bai, J. Dan, J. Yang, K. Zhou, X. Zhao, S. J. Pennycook and Z. Liu, *Adv. Mater.*, 2019, **31**, 1900862.

26 P. Li, J. Cui, J. Zhou, D. Guo, Z. Zhao, J. Yi, J. Fan, Z. Ji, X. Jing, F. Qu, C. Yang, L. Lu, J. Lin, Z. Liu and G. Liu, *Adv. Mater.*, 2019, **31**, 1904641.

27 Y. Deng, P. Li, C. Zhu, J. Zhou, X. Wang, J. Cui, X. Yang, L. Tao, Q. Zeng, R. Duan, Q. Fu, C. Zhu, J. Xu, F. Qu, C. Yang, X. Jing, L. Lu, G. Liu and Z. Liu, *ACS Nano*, 2021, **15**, 11526.

28 X. Qian, J. Liu, L. Fu and J. Li, *Science*, 2014, **346**, 1344.

29 M. N. Ali, J. Xiong, S. Flynn, J. Tao, Q. D. Gibson, L. M. Schoop, T. Liang, N. Haldolaarachchige, M. Hirschberger, N. P. Ong and R. J. Cava, *Nature*, 2014, **514**, 205.

30 H. Kwon, T. Jeong, S. Appalakondaiah, Y. Oh, I. Jeon, H. Min, S. Park, Y. J. Song, E. Hwang and S. Hwang, *Nano Res.*, 2020, **13**, 2534.

31 Y.-G. Choi, M.-H. Doan, L. L. P. Ngoc, J. Lee, G.-M. Choi and M. N. Chernodub, *Small*, 2023, **19**, 2206604.

32 Y. Yan, X. Zhang, X. Li, H. Fang, Y. Jiang and C. Zhao, *Adv. Funct. Mater.*, 2023, **33**, 2213933.

33 J.-X. Li, W.-Q. Li, S.-H. Hung, P.-L. Chen, Y.-C. Yang, T.-Y. Chang, P.-W. Chiu, H.-T. Jeng and C.-H. Liu, *Nat. Nanotechnol.*, 2022, **17**, 721.

34 Z. Zhang, Y. Liu, C. Dai, X. Yang, P. Chen, H. Ma, B. Zhao, R. Wu, Z. Huang, D. Wang, M. Liu, Y. Huangfu, S. Xin, J. Luo, Y. Wang, J. Li, B. Li and X. Duan, *Chem. Mater.*, 2021, **33**, 1307.

35 P. Yu, J. Lin, L. Sun, Q. L. Le, X. Yu, G. Gao, C.-H. Hsu, D. Wu, T.-R. Chang, Q. Zeng, F. Liu, J. Wang, H.-T. Jeng, H. Lin, A. Trampert, Z. Shen, K. Suenaga and Z. Liu, *Adv. Mater.*, 2017, **29**, 1603991.

36 P. E. Blöchl, *Phys. Rev. B: Condens. Matter Mater. Phys.*, 1994, **50**, 17953.

37 G. Kresse and J. Furthmüller, *Phys. Rev. B: Condens. Matter Mater. Phys.*, 1996, **54**, 11169.

38 G. Kresse and J. Furthmüller, *Comput. Mater. Sci.*, 1996, **6**, 15.

39 J. P. Perdew, K. Burke and M. Ernzerhof, *Phys. Rev. Lett.*, 1996, **77**, 3865.

40 G. Henkelman, B. P. Uberuaga and H. Jónsson, *J. Chem. Phys.*, 2000, **113**, 9901.

41 M. Küpers, P. M. Konze, S. Maintz, S. Steinberg, A. M. Mio, O. Cojocaru-Mirédin, M. Zhu, M. Müller, M. Luysberg, J. Mayer, M. Wuttig and R. Dronskowski, *Angew. Chem., Int. Ed.*, 2017, **56**, 10204.

42 M. Pisarra, C. Diaz and F. Martin, *Phys. Rev. B*, 2021, **103**, 195416.

43 H. Huang, X. Fan, D. J. Singh, H. Chen, Q. Jiang and W. Zheng, *Phys. Chem. Chem. Phys.*, 2016, **18**, 4086.

44 P. Zhang, P. Li, Q. Ma, M. Shen, Z. Tian and Y. Liu, *Appl. Surf. Sci.*, 2023, **623**, 157022.

45 M. M. Ugeda, A. Pulkin, S. Tang, H. Ryu, Q. Wu, Y. Zhang, D. Wong, Z. Pedramrazi, A. Martín-Recio, Y. Chen, F. Wang, Z.-X. Shen, S.-K. Mo, O. V. Yazyev and M. F. Crommie, *Nat. Commun.*, 2018, **9**, 3401.

46 J. Lin, J. Zhou, S. Zuluaga, P. Yu, M. Gu, Z. Liu, S. T. Pantelides and K. Suenaga, *ACS Nano*, 2018, **12**, 894.
47 L. Muechler, W. Hu, L. Lin, C. Yang and R. Car, *Phys. Rev. B*, 2020, **102**, 041103.
48 M. Yamamoto, S. T. Wang, M. Ni, Y.-F. Lin, S.-L. Li, S. Aikawa, W.-B. Jian, K. Ueno, K. Wakabayashi and K. Tsukagoshi, *ACS Nano*, 2014, **8**, 3895.
49 B. Peng, H. Zhang, W. Chen, B. Hou, Z.-J. Qiu, H. Shao, H. Zhu, B. Monserrat, D. Fu, H. Weng and C. M. Soukoulis, *npj 2D Mater. Appl.*, 2020, **4**, 14.
50 V. L. Deringer, W. Zhang, M. Lumeij, S. Maintz, M. Wuttig, R. Mazzarello and R. Dronskowski, *Angew. Chem., Int. Ed.*, 2014, **53**, 10817.
51 L. Chen, A. Y. Cui, M. Li, S. B. Li, S. J. Gong, K. Jiang, J. Z. Zhang, L. Q. Zhu, L. Y. Shang, Y. W. Li, Z. G. Hu and J. H. Chu, *Phys. Rev. B*, 2022, **106**, 214110.
52 X.-H. Lv, M.-Q. Wu, Y.-T. Ren, R.-N. Wang, H. Zhang, C.-D. Jin, R.-Q. Lian, P.-L. Gong, X.-Q. Shi and J.-L. Wang, *Phys. Rev. B*, 2022, **105**, 024108.
53 X. Zhou, H. Shu, Q. Li, P. Liang, D. Cao and X. Chen, *J. Mater. Chem. C*, 2020, **8**, 4432.
54 Z. Du, S. Yang, S. Li, J. Lou, S. Zhang, S. Wang, B. Li, Y. Gong, L. Song, X. Zou and P. M. Ajayan, *Nature*, 2020, **577**, 492.
55 D. A. Rehn, Y. Li, E. Pop and E. J. Reed, *npj Comput. Mater.*, 2018, **4**, 2.
56 G. Makov and M. C. Payne, *Phys. Rev. B: Condens. Matter Mater. Phys.*, 1995, **51**, 4014.
57 M. Leslie and N. J. Gillan, *J. Phys. C: Solid State Phys.*, 1985, **18**, 973.
58 H. Huang, X. Fan, D. J. Singh and W. Zheng, *Nanoscale*, 2020, **12**, 1247.
59 Y. T. Yan, L. Y. Chen, K. Dai, Y. F. Li, L. Wang, K. Jiang, A. Y. Cui, J. Z. Zhang and Z. G. Hu, *J. Phys. Chem. Lett.*, 2023, **14**, 7618.
60 J. Xia, D.-F. Li, J.-D. Zhou, P. Yu, J.-H. Lin, J.-L. Kuo, H.-B. Li, Z. Liu, J.-X. Yan and Z.-X. Shen, *Small*, 2017, **13**, 1701887.
61 K. A. N. Duerloo, Y. Li and E. J. Reed, *Nat. Commun.*, 2014, **5**, 4214.
62 S. Song, D. H. Keum, S. Cho, D. Perello, Y. Kim and Y. H. Lee, *Nano Lett.*, 2016, **16**, 188.